The near infrared cavity-enhanced absorption spectrum of methyl cyanide

Deirdre M. O'Leary[a,1], Albert A. Ruth[a,b,*], Sophie Dixneuf[a,b,2], Johannes Orphal[c,3], and Ravi Varma[a,4]

[a] Physics Department, University College Cork, Cork, Ireland.

[b] Environmental Research Institute (ERI), University College Cork, Cork, Ireland.

[c] Laboratoire Interuniversitaire des Systèmes Atmosphériques (LISA), CNRS UMR 7683, 94010 Créteil Cedex, France.

*Corresponding author: phone: +353-21-4902057, fax: +353-21-4276949, e-mail: a.ruth@ucc.ie

Abstract The absorption spectrum of methyl cyanide (CH_3CN) has been measured in the near IR between 6000 and 8000 cm^{-1} with a resolution of 0.12 cm^{-1} using Fourier transform incoherent broadband cavity-enhanced absorption spectroscopy. The spectrum contains several only weakly perturbed spectral regions; potential vibrational combination bands contributing to the spectrum are outlined. Line positions and cross-sections of CH_3CN between 6814 and 7067 cm^{-1} have been measured at high-resolution of 0.001 cm^{-1} using diode laser based off-axis cavity-enhanced absorption spectroscopy. A total of 4630 new absorption lines of CH_3CN are identified in this region. A value for the self-broadening coefficient has determined to be $(3.3 \pm 0.2) \times 10^{-3}$ cm^{-1} $mbar^{-1}$ for one isolated line at 7034.171 cm^{-1}. Several line series have been identified in these regions and an autocorrelation analysis performed with a view to aiding future assignments of the rotational-vibrational transitions.

Keywords Methyl cyanide, acetonitrile, Fourier transform cavity-enhanced spectroscopy, broadband absorption, high resolution.

1. Introduction

Methyl cyanide (CH_3CN, see Fig. 1) is a simple organic nitrile (acetonitrile), which, as a polar aprotic solvent is of common interest in industrial processes; e.g. for the determination of pesticide residues [3]. In the atmosphere methyl cyanide occurs as a trace constituent mainly as a result of biomass burning [4]–[6] and, to an extent, due to industrial processes and traffic [6]–[8]. It has been detected by remote sensing [9]–[13] and *in-situ* in surface air [14], in the troposphere [10], [15], and in the stratosphere [16]–[18] with typical mixing ratios ranging from the low pptv region in the upper stratosphere [13], [19], [20] to many ppbv in the vicinity of bushfires [15]. It is generally accepted that

[1] Present address: St. Luke's Radiation Oncology Network, St. Luke's Hospital, Rathgar, Dublin 6, Ireland.

[2] Present address: Forschungszentrum Jülich GmbH, IEK-8 (Troposphere), 52425 Jülich, Germany.

[3] Present address: Karlsruhe Institute of Technology, Institute for Meteorology and Climate Research (IMK), 76344 Eggenstein-Leopoldshafen, Germany.

[4] Present address: Physics Department, National Institute of Technology Calicut, Calicut, 673601 Kerala, India.

CH_3CN has a long lifetime in the atmosphere (> 6 months [10]). Removal of CH_3CN is mainly based on reaction with OH, but also oceanic losses and washout by rain have been suggested as effective sinks of atmospheric CH_3CN [10], [12], [17].

Methyl cyanide is also of considerable importance in astrophysics. The main isotopic species was first detected in the interstellar medium by Solomon *et al.* in 1971 [21]. The main isotopologue and other isotopic species have since been observed in numerous regions in the interstellar medium [22]–[26], in comets [27], [28], and in nearby galaxies [29], as well as in the atmosphere of Saturn's largest moon, Titan [30]–[34] (e.g. substantial mixing ratios of (1.4 – 1.5) × 10^{-6} for CH_3CN were reported on Titan below 1050 km by the Ion Neutral Mass Spectrometer aboard the Cassini mission). In diverse astrophysical topics [35]–[38] methyl cyanide is deemed a good spectroscopic probe of physical conditions such as temperature and density. One of the reasons for this significant interest in methyl cyanide by astronomers is the fact that it was one of the first molecules investigated by microwave spectroscopy and it is therefore one of the best studied symmetric top molecules. It has been the subject of a large number of laboratory studies to measure line positions and to determine spectroscopic assignments in the infrared. It has been also used as a probe molecule for special spectroscopic techniques such as Beam Maser spectroscopy [39], [40] and Laser Stark spectroscopy [41]:

Methyl cyanide is a prolate symmetric top molecule of C_{3v} symmetry (see Fig. 1). It has 12 normal modes of vibration; four non-degenerate vibrations of a_1-symmetry and four doubly-degenerate vibrations of *e*-symmetry. All vibrational modes are infrared and Raman active. Its ground state rotational structure has been studied in the far infrared between 7 and 60 cm^{-1} [42]. 1400 pure rotational transitions were identified, and assignments up to $J = 90$ and $J = 79$ were obtained in the ground and $\nu_8 = 1$ states respectively. Pavone *et al.* [43] investigated the ground state of CH_3CN by CO_2 laser difference frequency spectroscopy in the region 0.5 – 1.5 THz. Fundamentals, overtones and combination bands at low energies have been measured at high resolution in the mid infrared [44]–[49]. The $2\nu_8$ overtone band was studied using Fourier transform spectroscopy (FTS) [44] where 1000 lines could be assigned. Antilla *et al.* [45] studied the ν_5 fundamental, the $\nu_7 + \nu_8$ combination band and the $\nu_7 + \nu_8 - \nu_8$ hot band to obtain the ground state constants. Tolonen *et al.* [46] assigned 4000 lines to the ν_4, ν_7 and $3\nu_8$ bands. Paso *et al.* [47] took FTS data in the region between 1240 and 1650 cm^{-1} and assigned 3900 lines to the ν_6 and $\nu_7 + \nu_8$ bands. High resolution (0.0025 cm^{-1}) measurements of the ν_4 and ν_7 fundamental bands of CD_3CN are described in Ref. [48]. The ν_1 and ν_5 fundamental bands of CH_3CN were measured by Huet [49] between 2370 and 3500 cm^{-1}. 1700 lines were assigned to these bands. The high relevance of CH_3CN is also demonstrated by two recent publications on FT absorption spectroscopy by Harrison and Bernath [50] and Allen *et al*. [51], who measured air-broadened infrared absorption spectra of CH_3CN in the region 880 – 1700 cm^{-1} and around 3 μm with a resolution of 0.015 cm^{-1}. In [50], [51] cross-sections (for a range of temperatures; 207 – 297 K) were established with a multi-pass cell with a maximum path-length of 19.3 m.

The study of methyl cyanide has also recently been extended into the near infrared region by Rinsland *et al.* [52]. This study reports absorption cross-sections and integrated band intensities for spectra of CH_3CN measured in the laboratory. Spectra were recorded at a resolution of 0.112 cm^{-1}, at three temperatures in the wavenumber range 600 –

6500 cm^{-1}. The ν_4 parallel band (~920 cm^{-1}) was also comprehensively studied by Rinsland *et al.* [53]. In Ref. [53] the room temperature line positions and intensities for over 700 individual lines are reported together with nitrogen- and self-broadening coefficients as well as pressure induced line shift coefficients. In 2008 methyl cyanide has been added for the first time to the high-resolution transmission molecular absorption database (HITRAN, a compilation of molecular spectroscopic parameters for the simulation of transmission and emission of light in the atmosphere, www.cfa.harvard.edu/hitran) [54]. Based on data in Ref. [53] and supplemented by unpublished data [53] a total of 3572 absorption features are now available in HITRAN. Parameters on self- and air-broadened line widths have also been provided in Ref. [53].

High resolution absorption measurements at even higher ground state energies (>6500 cm^{-1}) are experimentally challenging due to increasingly weak transitions in this spectral region. In this work high resolution absorption data of CH_3CN in the ground state have been measured beyond 6000 cm^{-1} using two different cavity-enhanced approaches:

(a) *Fourier transform incoherent broadband cavity-enhanced absorption spectroscopy* (FT-IBBCEAS) using a supercontinuum light source [55], [56] to establish overview spectra at medium resolution between 6000 and 8000 cm^{-1}.

(b) *Off-axis cavity-enhanced absorption spectroscopy* (CEAS) [57] using an external cavity diode laser to establish a list of line positions and intensities in the near infrared region of the spectrum between 6814 and 7067 cm^{-1}.

The new absorption data of CH_3CN presented here are useful for the development of theoretical models of the ground state potential of CH_3CN and also potentially useful for future observation of CH_3CN using near infrared spectroscopy in astronomical studies.

2. Experimental

2.1. Off-axis cavity enhanced absorption setup

The experimental off-axis CEAS set-up is essentially the same as the one described in [58], [59]. The length of the optical cavity (Layertec mirrors: $r = -2$ m, $R \sim 0.997$) was 113 cm and the volume enclosed by the sample chamber was approximately 2 dm^3. An off-axis alignment of the optical cavity was employed to reduce the effect of the cavity's mode structure on the transmitted intensity. The incident beam entered the cavity at a distance of approximately 8 mm from the optical axis. The laser was typically scanned mode-hop free over 2 cm^{-1} per spectrum. The signal transmitted by the cavity was detected by an auto-balanced InGaAs photoreceiver (detector Nirvana 2017, New Focus) and averaged over 2000 sweeps per spectrum. This resulted in a 1σ noise level of 1.02×10^{-25} cm^2 $molecule^{-1}$ and a maximum signal-to-noise ratio of approximately 375. More than 200 spectra were concatenated to cover the overall spectral range reported.

2.2. Fourier transform incoherent broadband cavity-enhanced absorption setup

The experimental FT-IBBCEAS set-up is essentially the same as the one described in [56]. The optical cavity was attached to a vacuum chamber consisting of a long stainless steel pipe (100 mm diameter) which was pumped by a molecular turbo pump to approximately 1×10^{-5} mbar before introducing the sample gas. The length of the optical cavity (Layertec mirrors: r = –50 m, R ~ 0.999) was 644 cm. A supercontinuum (SC) fibre laser (Fianium, SC450, 6W) was used as light source. This pulsed source operates at 80 MHz delivering pulses of ~5 ps duration. Despite the higher brightness and better coupling efficiency of the SC source, due to low divergence and good spatial coherence in comparison to an arc lamp or light emitting diode, it was found that there was virtually no improvement of the signal to noise ratio when compared to the 'super quiet' Xe arc lamp (Hamamatsu) used in [56]. Even though the noise of the SC source was not quantified, the pulse-to-pulse intensity fluctuations of the source as a function of wavelength must be substantial. This fact is particularly severe because the light exiting the cavity was coupled into a FT spectrometer (Bruker, Vertex 80) supplied with a InGaAs photodiode sensor. In combination with an FT detection scheme the noise of the light source is fully transferred to the detector as opposed to an approach where light dispersion is used to determine the wavelength. Data were recorded at a resolution of 0.12 cm^{-1}.

2.3. Wavelength calibration and accuracy

The presence of a large number of H_2O absorption features due to minute quantities of water vapour in the sample chamber allowed for the absolute calibration of the wavenumber scale over a wide spectral region. The line positions of transitions in water [60] were taken from the HITRAN database [54]. The uncertainty of the positions is quoted as being between 0.001 and 0.01 cm^{-1}. In regions containing an insufficient number of water absorption lines, separate measurements were performed with a small quantity of a calibrating gas, CO_2 or NH_3, in the CEA chamber. The positions of the absorption lines of CO_2 [61] were also obtained from the HITRAN database [54]. The uncertainty in the positions of CO_2 lines is quoted as being between 0.0001 and 0.001 cm^{-1}. The positions of NH_3 lines, taken from [58], had an uncertainty of 0.001 cm^{-1}. Absorption by CH_3CN and the calibration gas was recorded simultaneously thereby enabling the absolute wavenumber calibration of CH_3CN lines over the entire spectral region covered. Calibration was performed by position interpolation over the whole wavenumber scale and subsequent linear regression. The standard deviation of the fit parameters enabled an estimation of the uncertainty of the line positions at between 0.005 cm^{-1} and 0.01 cm^{-1}.

2.4. Calibration of the mirror reflectivity

In order to determine absorption coefficients and cross-sections with CEAS, it is necessary to know the reflectivity of the cavity mirrors over the whole range of measurement. The reflectivity of the mirrors is determined by measuring the absorption of a known amount of CO_2, whose line intensities are well known. The HITRAN database lists line intensities, i_H, [1/ (cm × molecule × cm^{-2})] as the integral of the absorption cross-sections at a temperature of 296 K.

The reflectivity, R, may be obtained from the line intensity i_H as follows:

$$R = 1 - \frac{N\,d\,i_H}{\int\left(\frac{I_0(\tilde{\nu})}{I(\tilde{\nu})} - 1\right)\mathrm{d}\tilde{\nu}} \tag{1}$$

where N [molecule × cm^{-3}] is the number density of the calibration gas (CO_2), d [cm] is the cavity length, and I and I_0 are the transmitted intensities with and without the calibration gas, respectively. The absorption by CO_2 was examined between 6870 and 6990 cm^{-1} for the CEAS experiment and between ~6460 and ~7760 cm^{-1} for the FT-IBBCEAS experiment. The error associated with other parameters such as the length of the cavity, the pressure of the sample and the integrated area under an absorption peak (denominator in (1)) is small so that the uncertainty in R is dominated by the error in the line intensities of the CO_2 lines. This error is quoted by HITRAN to be between 5% and 10%. The associated error in the value of (1-R) was therefore estimated to be 10%. A graph of the mirror reflectivity spectra obtained from the CO_2 measurements for the two sets of mirrors used in this work is presented in Fig. 2.

2.5. Materials and Gas preparation

Pressures of 4-5 mbar of CH_3CN was chosen to enable the observation of weak absorption features while still trying to minimize the effect of line broadening, and associated blending of absorption features, in the observed spectrum. The acetonitrile sample (Labscan Analytical Sciences, Spectroscan grade) had a quoted purity of 99.9% (GC assay). The maximum impurity level of water in the solvent was stated at 0.05%. Degasification of the CH_3CN sample was carried out by performing a number of 'freeze-pump-thaw' cycles.

2.6. Water absorption feature and their elimination

The presence of water inside the cavity and in the beam path outside the cavity resulted in the presence of unwanted water absorption features in the spectra which potentially completely obscure any CH_3CN absorption. Rigorous water removal strategies were therefore necessary. Prior to experiments, the stainless steel chambers in both experiments were cleaned extensively with HPLC grade acetone. The sample chambers were evacuated for several days using a turbo molecular pump before the commencement of the absorption measurements. Although no significant leakage of air into the evacuated sample volume was noted, the 'growth' of water absorption features was observed with time, which was caused by desorption of water vapour from the walls of the sample chamber. In order to remove the water in the lab air outside the cavity it was necessary to place a plastic cover around the experiments, enclosing the optical path where possible. The volume inside of the plastic cover was purged with either dried compressed air or nitrogen gas. In case of the FT-IBBCEAS experiments the FT spectrometer was constantly flushed with dried and filtered lab air. In the case of the CEAS experiments purge gases were passed through a P_2O_5 trap to further remove any traces of water. Despite these measures water features could only be dramatically reduced but not entirely suppressed experimentally. The presence of the large number of water absorption lines (see section III.*A*.)

was thus used for direct calibration of the wavenumber scale. It should be noted, that only water absorption lines that are unaffected by saturation and arising from water inside the cavity were used to calibrate the wavenumber scale.

3. Results and discussion

3.1. FT-IBBCEAS overview spectra

Fig. 3 (black trace) shows an overview spectrum of CH_3CN (4 mbar) between 6000 and 8000 cm^{-1}, measured with a resolution of 0.12 cm^{-1} in an acquisition time of 60 min. The data file can be found in the electronic supplementary material. The absorption lines in this region are extremely weak and have not been addressed experimentally before in the gas phase. Several regions of strongly overlapping vibrational combination bands occur in the spectrum, whose structure is not rotationally resolved. In some cases distinct P- or R-branches can be identified. The strongest band in the entire spectrum occurs between 6000 and 6150 cm^{-1}, where the first harmonic overtones $2\nu_1$ and $2\nu_5$ can occur as well as $\nu_1+\nu_5$. This region represents a "classic" perpendicular band of a symmetric top molecule where the strongest features correspond to individual Q-branches (also see [52], [53]). A list of potentially occurring vibrational states in the region between ~6150 and 7500 cm^{-1} is given in Table I for the combination of three fundamental modes only (Note: the values in Table I are purely combinatorial and do not take the anharmonicity of the molecule into account – they must not be read as assignments in this region). Based on the absorption strength of the fundamentals [62], [63], the combinations that would be expected to contribute the strongest to the observed spectrum are highlighted in Table I. Due to the strong coupling of vibrational modes and the high congestion of the spectrum, a comprehensive analysis of the data cannot be easily performed. It is interesting, however, that the spectrum behaves relatively "normal" in this region and does not exhibit an overly complex (e.g. polyad) structure. An approach to the analysis based on anharmonic force field calculations [64] rather than harmonically coupled local modes, as presented by Ahmed and Henry [65] for measurement in the liquid phase in this region, may already describe the spectrum obtained at a satisfactory level. Above 7500 cm^{-1} a significant decrease in the CH_3CN absorption is observed (see Fig. 4). Between 7500 and 8000 cm^{-1} only the absorption of states consisting of a combination of at least four vibrational quanta contribute to the spectrum. The spectrum is highly congested and exhibits several complex vibrational band systems that cannot be resolved with the present setup. Overtone combination bands above 8000 cm^{-1} have only been addressed at low resolution in the liquid phase, where inhomogeneous broadening dominates the line profiles [65], [66].

The spectrum in Fig. 3 also contains absorption lines that are due to H_2O. The corresponding lines can be identified on basis of the HITRAN database [54] (blue trace in Fig. 3 shown for comparison). The spectrum also contains (rotationally resolved) absorption features based on the impurity HCN. The HCN feature is based on the CH-stretch overtone $2\nu_3$ with band centre at $\approx$6520 cm^{-1} [67]. The HCN band in the spectrum was the only feature whose relative absorption appeared to vary time dependently from measurement to measurement. Its occurrence

could never be entirely avoided. The green trace in Fig. 3 shows the region which was additionally recorded with high-resolution off-axis CEAS (see Fig. 5) – it will be discussed in section III.*B*.

Fig. 3 and 4 demonstrate the advantage of combining IBBCEAS with a Fourier transform detection scheme. A large spectral region can be covered at a resolution which is relevant for air-broadened lines under normal conditions. The 1σ noise based on data at 7625±25 cm^{-1} is approximately 1×10^{-8} cm^{-1} (60 min acquisition time). Despite the significant spectral and temporal noise of the supercontinuum source the signal-to-noise (SNR) ratio above 7500 cm^{-1} is still ~60; in the region around 6000 cm^{-1}, where the absorption signal is close to saturation, the SNR can approach 10^5.

3.2. Off-axis CEAS high resolution spectra

The cavity-enhanced absorption spectrum of methyl cyanide, recorded at a pressure of 5 mbar is shown in Fig. 5. Approximately 200 individual, overlapping spectral segments were concatenated to cover a spectral range of approximately 250 cm^{-1}. The recorded spectrum of CH_3CN is very dense – 4630 new absorption transitions of methyl cyanide were identified corresponding to an average density of 18 lines per cm^{-1}. The rotational structure of the spectrum is in many parts not fully resolved. The largest absorption signal was detected at 6930.962 cm^{-1}. The absorption cross-section of this line is 6.54×10^{-23} cm^2 with a corresponding absorption coefficient of 8.14×10^{-6} cm^{-1}. The lowest detectable peak was measured at 6914.257 cm^{-1} with an absorption cross-section of 5.18×10^{-25} cm^2 and an absorption coefficient of 6.45×10^{-8} cm^{-1}. A comprehensive list of line positions and absorption strengths of CH_3CN obtained using CEAS is given in the supplementary material.

Since the spectrum of methyl cyanide was measured at 5 mbar, the effect of pressure broadening (see section III.*C*.) causes adjacent lines to blend into one another. Therefore zero-absorption was not always well defined. In each of the measured spectral segments a program was used to locate the positions of absorption minima which were assumed to be zero. A polynomial was then fitted through all of these positions to determine the zero-absorption baseline over the entire spectral segment.

Despite the efforts to remove water from the spectrum (see section II.*F*.) it was still necessary to identify the strongest H_2O lines by comparison with the HITRAN 2004 database and remove them from the CH_3CN absorption spectrum. As an example the spectral interval between 6990 and 7000 cm^{-1}, measured with off-axis CEAS and FT-IBBCEAS, is shown in Fig. 6. The water features (represented in form of a blue "stick spectrum" based on the HITRAN integrated line data in this region) have been removed from the spectrum. Fig. 6 illustrates the importance of minimizing and removing the water absorption features from the spectrum.

Spectral analysis

The possible overtone and combination bands for absorption transitions, up to three quanta, in the region between 6800 and 7100 cm^{-1} are listed in Table I. Since intensities of overtones and combination bands strongly decrease with increasing number of quanta [68], the bands considered in Table I only consist of three quanta. All vibrational

transitions in Table I are symmetry allowed. The overview spectrum in Fig. 5 was (somewhat arbitrarily) subdivided into three regions which will be discussed in turn:

Region (i): 6814 – 6900 cm^{-1}

There are approximately 20 absorption transitions per cm^{-1} in this region and several spectral series provide evidence of band structure. Fig. 7(a) shows an example of a series of 13 absorption lines between 6875 and 6885 cm^{-1} with equidistant energy separation of 0.66 cm^{-1}. As a prolate symmetric top molecule (moment of inertia $I_c = I_b > I_a$, cf. insert Fig. 5) CH_3CN may display equidistant line series for modes of motion were centrifugal distortion is negligible. The line separation $\Delta\tilde{\nu} = 2B$ depends on the rotational constant, B, which was stated as 0.3068 cm^{-1} in [49]. The value for $2B$ matches the separation of the strong lines in Fig. 7(a) by ≈0.05 cm^{-1}. An autocorrelation of the corresponding spectral region between ~6876 and 6885 cm^{-1} was performed and is exemplified in Fig. 7(b). The autocorrelation $A_c(\zeta)$ of the wavenumber-dependent absorption coefficient, $\alpha(\tilde{\nu})$, is a mathematical tool to identify repeating patterns in the spectrum. A_c is essentially the cross-correlation of $\alpha(\tilde{\nu})$ with itself at a lag ζ [69]:

$$A_c(\zeta) = \int_{-\infty}^{\infty} \alpha(\tilde{\nu})\alpha(\tilde{\nu} - \zeta)\, d\tilde{\nu}\,. \qquad (2)$$

The wavenumber differences, $\Delta\tilde{\nu}$, for the two most significant peaks obtained from the autocorrelation correspond to 0.68 cm^{-1} and 1.30 cm^{-1} (vertical arrows in Fig. 7(b)). These two values (No. 1 and 2 in Table II) can be considered fundamental and second harmonic spacings of the series, respectively. The error in the positions of the peaks was estimated empirically by fitting a number of Gaussian profiles to the background-subtracted peaks of the autocorrelation curve. The FWHM of the Gaussian closest to the maximum of the autocorrelation peak was used as an estimate of the error. Other reasonably undisturbed line series were identified in the spectrum and a list of dominant equidistant separations based on similar analyses in other spectral regions is shown in Table II. In Table II the values for $\Delta\tilde{\nu}$ obtained from the autocorrelation are compared with those determined from repeating patterns of lines in the spectrum. Additionally the position of each line in Fig. 7(a) was plotted versus a corresponding (relative) quantum number J, which was arbitrarily assigned to each position. A linear regression was applied to the data as shown in Fig. 7(b) (red line) in order to retrieve an estimate of $2B$ based on the assumption of negligible higher order vibration-rotation interactions. The quadratic nature of the residuals of the linear fit exhibit the effect of centrifugal distortion on the rotational energy levels as outlined in Fig. 7(c). The maximum error in the peak positions is ~0.01 cm^{-1} and lies within the symbol size of data points in Fig. 7(c). The observed deviations in the residuals are therefore significant and real. A second order polynomial was used as a fit function corroborating the fact that this series is weakly distorted by the presence of vibration-rotation interactions. The linear regression approach was used in the following analysis in other parts of the spectrum in order to retrieve values for $\Delta\tilde{\nu}$ and indeed other wavenumber intervals of interest. For instance, a similar series of lines was identified in the region between 6865 and 6871 cm^{-1} (Table II).

Region (ii): 6900 – 7005 cm^{-1}

This region of the spectrum contains the lines of greatest absorption cross-section. The density of absorption features in this region is approximately 7 transitions per cm^{-1} based on a peak counting approach. Potential vibrations occurring in this region of the spectrum are the combination bands $\nu_4 + 2\nu_5$, $2\nu_1 + \nu_7$ and $\nu_1 + \nu_5 + \nu_7$. These transitions have *e*-symmetry and result in perpendicular bands. The selection rule $\Delta K = \pm 1$ for perpendicular bands allows *Q* branches to be spectrally displaced relative to one another. The separation of successive *Q* branches in different perpendicular bands of a given symmetric top molecule may vary considerably [68]. The band shape is strongly dependent on the vibration-rotation (Coriolis) interaction, hence the band appearance can vary from regular *P*, *Q*, *R* branches structure to structureless. In the region considered here no regular *P*, *Q*, *R*-band structures or obvious band centres were observed. Features consisting of many closely spaced absorption transitions amalgamated together are prevalent and probably correspond to band heads of *Q* branches of perpendicular bands. An example of such a feature is given in Fig. 8. Six of these strongly blended absorption features were noted in the region between 6975 and 7005 cm^{-1}. They are approximately equidistantly spaced with a mean separation of 5.4 ± 0.1 cm^{-1}, suggesting that these features form part of a spectral series which is governed by the the rotational *A* constants, which is known to be 5.27 cm^{-1} [53].

Region (iii): 7005 – 7067 cm^{-1}

This region of the spectrum is quite densely populated with an average of ca. 18 absorption transitions per cm^{-1}. Considering up to three quanta, the only vibration that can occur in this region is the $2\nu_5 + \nu_7$ combination band. The region exhibits distinct spectral patterns particularly in the range between 7020 and 7060 cm^{-1}. Seemingly unperturbed spectral patterns are readily identifiable in this region. For example, a pattern of 32 "double lines", separated by ≈0.2 cm^{-1} is repeating at intervals of approximately 0.63 cm^{-1} in the region between 7020 and 7040 cm^{-1}. Values corresponding to an autocorrelation of the spectrum between 7027 and 7032 cm^{-1} is shown in Table II. The four respective entries (No. 5…8) correspond to the four possible line separations of two adjacent double lines. The two values of the repetition interval (denoted a and b in the third column of Table II) were calculated by considering both lines of the doublet. A second series of seemingly unperturbed double lines is identified in the region between 7048 and 7060 cm^{-1}. The two strongly absorbing transitions are displaced by approximately 0.28 cm^{-1} relative to one another. An autocorrelation of the spectral region between 7049 and 7054 cm^{-1} was obtained showing three significantly broadened features (Table II, No. 9…11). The values $\Delta\tilde{\nu}$ correspond to the separation of the double lines, the repetition interval of the pattern, and the sum of both. In this pattern the second line of the doublet lay approximately in the centre of the repetition interval. For this reason, two estimates of the doublet separation and the repetition interval (labeled c, d, e and f respectively in Table II) were obtained by examining the spectrum directly. This is also the reason why the peaks in the autocorrelation plot appear significantly broadened.

Unfortunately, spectral information in the region between 7040 and 7049 cm^{-1} was obscured owing to the presence of water vapour. It is conceivable that the origin of the vibrational combination band, $2\nu_5 + \nu_7$, lies within this region. Indeed the observed spacing of the repeating patterns at lower energies is greater than that observed for the patterns

at higher energies, suggesting that the observed lines belong to the corresponding *P* and *R* branches respectively.

Finally, in the regions between 7031 and 7034 cm^{-1} and 7058 and 7060 cm^{-1} series of lines were found in the spectrum consisting of line pairs where the separation between the lines gradually diminishes with increasing wavenumber.

3.3. Pressure broadening at 7034.17 cm^{-1}

The high density of absorption transitions in this spectrum makes it difficult to locate isolated lines for accurate measurements of line widths and pressure broadening parameters. An absorption transition at 7034.171 cm^{-1} was chosen for a line width and pressure broadening analysis, because it is reasonably well isolated from adjacent lines. Self-pressure broadening of methyl cyanide was investigated by fitting Voigt profiles to this line measured at different pressures of CH_3CN between 0.5 and 10 mbar. An example at 5 mbar is presented in the insert of Fig. 9 together with an associated Voigt profile fitted to the experimental data. The Voigt fit provided values of 0.01263 cm^{-1} and 0.0144 cm^{-1} for the Gaussian (ν_G) and Lorentzian FWHM (ν_L) values, respectively. There was no evidence of collisional narrowing – the absorption profiles are reasonably well reproduced by Voigt profiles – although such an effect may be masked by noisy data in this case. The theoretically expected Doppler FWHM was calculated to be 0.0135 cm^{-1}. The Lorentzian line width of the absorption line at 7034.171 cm^{-1} as a function of CH_3CN pressure is shown in Fig. 9. A linear fit to the data yielded a self-broadening coefficient of 3.28×10^{-3} cm^{-1} $mbar^{-1}$ with an intercept of -1.44×10^{-3} cm^{-1} (dashed line in Fig. 9). The main source of error leading to the small but non-zero intercept results from the contribution of lines next to 7034.171 cm^{-1} which affects the fit, particularly for larger pressures. In order to account for line blending effects from adjacent absorption transitions, Voigt profiles were also fitted to the adjacent lines during the fitting procedure. However, the uncertainty due to line overlap is significantly larger in comparison to the error in the pressure reading (± 0.01 mbar) and the inherent fit uncertainty, which is typically less than 5%. A second linear fit constrained to go through the origin was applied to the data (red straight line in Fig. 9) and yielded a self-broadening coefficient of 3.07×10^{-3} cm^{-1} $mbar^{-1}$. The difference between the two values of the self-broadening coefficient obtained was taken as the uncertainty in the value of the broadening coefficient. The self-broadening coefficient was therefore measured to be $(3.3 \pm 0.2) \times 10^{-3}$ cm^{-1} $mbar^{-1}$. This value for the self-broadening coefficient compares well to results obtained by Rinsland *et al.* who measured self-broadened half width coefficients as large as 2.0 cm^{-1} atm^{-1} [53].

CONCLUSIONS

Fourier transform incoherent broadband cavity-enhanced absorption spectroscopy (FT-IBBCESA) has been applied to measure the absorption spectrum of methyl cyanide (CH_3CN) between 6000 and 8000 cm^{-1} with a resolution of 0.12 cm^{-1}. The high energy region of the CH_3CN spectrum (>6500 cm^{-1}) has been addressed spectroscopically for the first time. Additionally, diode laser based off-axis cavity-enhanced absorption spectroscopy has been used to measure

line positions and cross-sections between 6814 and 7067 cm^{-1} with high resolution of 0.001 cm^{-1}. A total of 4630 new absorption lines of CH_3CN were identified in this region. The spectrum contains several only weakly perturbed spectral regions and potential vibrational combination bands contributing to the spectrum have been identified. Several line series have been identified in these regions and an autocorrelation analysis performed with a view to aiding future assignments of the rotational-vibrational transitions. The self-broadening of one isolated line at 7034.171 cm^{-1} has been studied and the corresponding broadening coefficient was determined as $(3.3 \pm 0.2) \times 10^{-3}$ cm^{-1} $mbar^{-1}$.

ACKNOWLEDGEMENT

The authors would like to thank Dr. Pascale Chelin (University Paris-Sud, Creteil, France) for her help with the FT measurements. The excellent technical assistance provided by J. Sheehan and C. Roche (Physics Department, UCC) is gratefully acknowledged.

This work was supported by the Irish EPA (STRIVE program, 2008-FS-EH-2-S5). D.M. O'Leary and S. Dixneuf received support through fellowships from the Irish Research Council for Science Engineering and Technology (EMBARK initiative 2005 (postgraduate programme) and 2008 (post-doctoral programme), respectively).

APPENDIX

The data files of the overview spectra shown in Figs. 3 and 5 are available in the supplementary material together with a list of resolved absorption lines in the region measured by off-axis CEAS.

REFERENCES

[1] Šimečková M, Urban Š, Fuchs U, Lewen F, Winnewisser G, Morino I, Yamada KMT. J. Mol. Spectrosc. 2004; 226:123–136.

[2] Anttila R, Horneman V-M, Koivusaari M, Paso R. J. Mol. Spectrosc. 1993; 157:198–207.

[3] Anastassiades M, Lehotay SJ, Stajnbaher D, Schenck FJ. Fast and easy multiresidue method employing acetonitrile extraction/partitioning and "dispersive solid-phase extraction" for the determination of pesticide residues in produce, J. AOAC Int. 2003; 86:412–431.

[4] Lobert JM, Scharffe DH, Hao WM, Crutzen PJ. Importance of biomass burning in the atmospheric budgets of nitrogen-containing gases. Nature 1990; 346:552–54.

[5] de Gouw JA, Warneke C, Parrish DD, Holloway JS, Trainer M, Fehsenfeld FC. Emission sources and ocean uptake of acetonitrile (CH_3CN) in the atmosphere. J. Geophys. Res.-Atmos. 2003; 108:D11 4329, doi: 10.1029/2002JD002897.

[6] Holzinger R, Jordan A, Hansel A, Lindinger W. Automobile emissions of acetonitrile: Assessment of its contribution to the global source. J. Atmos. Chem. 2001; 38:187–93.

[7] Arijs EJ, Brasseur G. Acetonitrile in the stratosphere and implications for positive ion composition. J. Geophys. Res. 1986; 91:4003–16.

[8] Hamm S, Warneck P. The interhemispheric distribution and the budget of acetonitrile in the troposphere. J. Geophys. Res. 1990; 95:20593–606.

[9] Carli B, Carlotti M. Far infrared and microwave spectroscopy of the Earth's atmosphere. in: "Spectroscopy of the earth's atmosphere and interstellar medium", Academic Press, New York, pp. 1–95, 1992.

[10] Singh HB, Salas L, Herlth D, Kolyer R, Czech E, Viezee W et al. In situ measurements of HCN and CH_3CN over the Pacific Ocean: Sources, sinks, and budgets. J. Geophys. Res.-Atmos. 2003; 108:8795, doi: 10.1029/2002JD003006.

[11] Livesey NJ, Waters JW, Khosravi R, Brasseur GP, Tyndall GS, Read WG. Stratospheric CH_3CN from the UARS microwave limb sounder. Geophys. Res. Lett. 2001; 28:779–82.

[12] Livesey NJ, Fromm MD, Waters JW, Manney GL, Santee ML, Read WG. Enhancements in lower stratospheric CH_3CN observed by the upper atmosphere research satellite microwave limb sounder following boreal forest fires. J. Geophys. Res.-Atmos. 2004; 109:D06308, doi: 10.1029/2003JD004055.

[13] Kleinböhl A, Toon GC, Sen B, Blavier JFL, Weisenstein DK, Wennberg PO. Infrared measurements of atmospheric CH_3CN. Geophys. Res. Lett. 2005; 32:L23807, doi: 10.1029/2005GL024283.

[14] Snider JR, Dawson GA. Surface acetonitrile near Tucson, Arizona. Geophys. Res. Lett. 1984; 11:241–42.

[15] Becker KH, Ionescu A. Acetonitrile in the lower troposphere. Geophys. Res. Lett. 1982; 9:1349–51.

[16] Arnold F, Bohringer H, Henschen G. Composition measurements of stratospheric positive-ions. Geophys. Res. Lett. 1978; 5:653–56.

[17] Schneider J, Bürger V, Arnold F. Methyl cyanide and hydrogen cyanide measurements in the lower stratosphere: Implications for methyl cyanide sources and sinks. J. Geophys. Res.-Atmos. 1997; 102:D21, doi: 10.1029/97JD02364.

[18] Arijs E, Nevejans D, Ingels J. Stratospheric positive-ion composition measurements and acetonitrile detection - a consistent picture. Int. J. Mass Spectr. Ion Process 1987; 81:15–31.

[19] Arnold F, Hauck G. Lower stratosphere trace gas detection using aircraft-borne active chemical ionization mass spectrometry. Nature 1985; 315:307–9.

[20] Knop G, Arnold F. Stratospheric trace gas detection using a new balloon-borne ACIMS method: acetonitrile, acetone, and nitric acid. Geophys. Res. Lett. 1987; 14:1262–65.

[21] Solomon PM, Jefferts KB, Penzias AA, Wilson RW. Detection of millimeter emission lines from interstellar methyl cyanide. Astrophys. J. 1971; 168:L107.

[22] Sutton EC, Blake GA, Masson CR, Phillips TG. Molecular line survey of Orion from 215 to 247 GHz. Astrophys. J. Suppl. Ser. 1985; 58:341–78.

[23] DeVicente P, Martin Pintado J, Wilson TL. A hot ring in the Sagittarius B2 molecular cloud. Astron. Astrophys. 1997; 320:957–71.

[24] Kalenskii SV, Promislov VG, Alakoz AV, Winnberg A, Johansson LEB. Probing the properties of methyl cyanide sources. Astron. Astrophys. 2000, 354:1036–40.

[25] Watson C, Churchwell E, Pankonin V, Bieging JH. Arcsecond images of CH_3CN toward W75N. Astrophys. J. 2002; 577:260–64.

[26] Araya E, Hofner P, Kurtz S, Bronfman L, DeDeo S. CH_3CN observations toward southern massive star-forming regions. Astrophys. J. Suppl. Ser. 2005; 157:279–301.

[27] Crovisier J. Physics and chemistry of comets: recent results from comets Hyakutake and Hale-Bopp - Answers to old questions and new enigmas. Faraday Discuss. 1998; 109:437–52.

[28] Biver N, Bockelee-Morvan D, Crovisier J, Lis DC, Moreno R, Colom P et al. Radio wavelength molecular observations of comets C/1999 T1 (McNaught-Hartley), C/2001 A2 (LINEAR), C/2000 WM1 (LINEAR) and 153P/Ikeya-Zhang. Astron. Astrophys. 2006; 449:1255–U1240.

[29] Mauersberger R, Henkel C, Walmsley CM, Sage LJ, Wiklind T. Dense gas in nearby galaxies. 5. multilevel studies of CH_3CCH and CH_3CN. Astron. Astrophys. 1991; 247:307–14.

[30] Bézard B, Marten A, Paubert G. Detection of acetonitrile on Titan. American Astronomical Society, 25th DPS Meeting (#25.09). Bull. Am. Astron. Soc. 1993; 25:1100.

[31] Marten A, Hidayat T, Biraud Y, Moreno R. New millimeter heterodyne observations of Titan: vertical distributions of nitriles HCN, HC_3N, CH_3CN, and the isotopic ratio $^{15}N/^{14}N$ in its atmosphere. Icarus 2002; 158:532–44.

[32] Lorentz R, Mitton J. Lifting Titan's veil: exploring the giant moon of Saturn. Cambridge: Cambridge University Press; 2002, p. 260.

[33] Coustenis A, Achterberg RK, Conrath BJ, Jennings DE, Marten A, Gautier D et al. The composition of Titan's stratosphere from Cassini/CIRS mid infrared spectra. Icarus 2007; 189:35–62.

[34] Cui J, Yelle RV, Vuitton V, Waite JH, Kasprzak WT, Gell DA et al. Analysis of Titan's neutral upper atmosphere from Cassini ion neutral mass spectrometer measurements. Icarus 2008; 200:581–615.

[35] Pearson JC, Müller HSP. The submillimeter wave spectrum of isotopic methyl cyanide. Astrophys. J. 1996; 471:1067–72.

[36] Cummins SE, Green S, Thaddeus P, Linke RA. The kinetic temperature and density of the sagittarius-B2 molecular cloud from observations of methyl cyanide. Astrophys. J. 1983; 266:331–38.

[37] Loren RB, Mundy LG. The methyl cyanide hot and warm cores in Orion - statistical equilibrium excitation models of a symmetric-top molecule. Astrophys. J. 1984; 286:232–51.

[38] Sutton EC, Blake GA, Genzel R, Masson CR, Phillips TG. Excitation of methyl cyanide in the hot core of Orion. Astrophys. J. 1986; 311:921–29.

[39] Kukolich SG, Lind G, Barfield M, Faehl L, Marshall JL. Carbon-13 magnetic shielding from beam-maser measurements of spin-rotation interaction in acetonitrile. J. Am. Chem. Soc. 1978; 100:7155–59.

[40] Kukolich SG. Beam maser spectroscopy on $J=1\rightarrow2$, $K=1$, and $K=0$ transitions in CH_3CN and (CH_3CN)-C-13. J. Chem. Phys. 1982; 76:97–101.

[41] Rackley SA, Butcher RJ, Römheld M, Freund SM, Oka T. Laser Stark spectroscopy of methyl cyanide in the 10 mm region: Analysis of the ν_4 and ν_7 bands, and the ν_7, $3\nu_8^1$ interaction. J. Mol. Spectr. 1982; 92:203–17.

[42] Carlotti M, Dilonardo G, Fusina L, Carli B. The far infrared spectrum of methyl cyanide, CH_3CN. J. Mol. Spectr. 1988; 129:314–25.

[43] Pavone FS, Zink LR, Prevedelli M, Inguscio M. Tunable FIR spectroscopy of CH_3CN between 569 GHz and 1.48 THz. J. Mol. Spectr. 1990, 144:45–50.

[44] Koivusaari M, Tolonen AM, Paso R, Schroderus J, Anttila R. The $2\nu_8$-band of CH_3CN. J. Mol. Spectr. 1993; 160:566–73.

[45] Anttila R, Horneman VM, Koivusaari M, Paso R. Ground-state constants a_0, D_{0K} and H_{0K} of CH_3CN. J. Mol. Spectr. 1993; 157:198–207.

[46] Tolonen AM, Koivusaari M, Paso R, Schroderus J, Alanko S, Anttila R. The infrared spectrum of methyl cyanide between 850 and 1150 cm^{-1} - analysis of the ν_4 - band, ν_7 - band, and $3\nu_8^1$-band with resonances. J. Mol. Spectr. 1993; 160:554–65.

[47] Paso R, Anttila R, Koivusaari M. The infrared spectrum of methyl cyanide between 1240 and 1650 cm^{-1} - the coupled band system ν_3, $\nu_{6\pm1}$, and $\nu_7+\nu_{8\pm2}$. J. Mol. Spectr. 1994; 165:470–80.

[48] Koivusaari M and Anttila R. The ν_4 and ν_7 bands of CD_3CN with Coriolis interaction and other perturbations. J. Mol. Spectr. 1992; 156:201–9.

[49] Huet TR. The ν_1 and ν_5 fundamental bands of methyl cyanide. J. Mol. Structure 2000; 517/518:127–31.

[50] Harrison JJ, Bernath PF. Mid- and long-wave infrared absorption cross-sections for acetonitrile. J. Quant. Spectr. Rad. Trans. 2011; doi: 10.1016/j.jqsrt.2011.11.003.

[51] Allen NDC, Harrison JJ, Bernath PF. Acetonitrile (CH_3CN) infrared absorption cross-sections in the 3 μm region. J. Quant. Spectr. Rad. Trans. 2011; 112:1961–66.

[52] Rinsland CP, Sharpe SW, Sams RL. Temperature-dependent infrared absorption cross-sections of methyl cyanide (acetonitrile). J. Quant. Spectr. Rad. Trans. 2005; 96:271–80.

[53] Rinsland CP, Devi VM, Benner DC, Blake TA, Sams RL, Brown LR et al. Multispectrum analysis of the ν4 band of CH_3CN: Positions, intensities, self- and N_2-broadening, and pressure-induced shifts. J. Quant. Spectr. Rad. Trans. 2008; 109:974–94.

[54] Rothman LS, Gordon IE, Barbe A, Benner DC, Bernath PE, Birk M et al. The HITRAN 2008 molecular spectroscopic database. J. Quant. Spectr. Rad. Trans. 2009; 110:533–72.

[55] Ruth AA, Orphal J, Fiedler SE. Cavity-enhanced Fourier transform absorption spectroscopy using an incoherent broadband light source. Appl. Opt. 2007; 46:3611–16.

[56] Orphal J, Ruth AA. High-resolution Fourier transform cavity-enhanced absorption spectroscopy in the near-infrared using an incoherent broad-band light source. Opt. Express 2008; 16:19232–43.

[57] Paul JB, Lapson L, Anderson JG. Ultrasensitive absorption spectroscopy with a high-finesse optical cavity and off-axis alignment. Appl. Opt. 2001; 40:4904–10.

[58] O'Leary DM, Orphal J, Ruth AA, Heitmann U, Chelin P, Fellows CE. The cavity-enhanced absorption spectrum of NH_3 in the near infrared region between 6850 and 7000 cm^{-1}. J. Quant. Spectr. Rad. Trans. 2008; 109:1004–15.

[59] Staak M, Gash EW, Venables DS, Ruth AA. The rotationally-resolved absorption spectrum of formaldehyde from 6547 to 6804 cm^{-1}. J. Mol. Spectr. 2005; 229:115–21.

[60] Toth RA. Extensive Measurements of (H_2O)-O-16 Line Frequencies and Strengths - 5750 to 7965 cm^{-1}. Appl. Opt. 1994; 33:4851–67.

[61] Miller CE, Brown LR. Near infrared spectroscopy of carbon dioxide I. $^{16}O^{12}C^{16}O$ line positions. J. Mol. Spectr. 2004; 228:329–54.

[62] Shimanouchi T. Tables of molecular vibrational frequencies. Consolidated Volume I, Nat. Stand. Ref. Data Ser., Nat. Bur. Stand. 1972, 39:1–160.

[63] Koga Y, Kondo S, Saeki S, Person WB. Infrared intensities of Acetonitrile. J. Phys. Chem. 1984; 88:3152–57.

[64] Begue D, Carbonniere P, Pouchan C. Calculations of vibrat-ional energy levels by using a hybrid *ab initio* and DFT quartic force field: application to acetonitrile. J. Phys. Chem. A 2005; 109:4611–16.

[65] Ahmed MK, Henry BR. Intensity distribution in the overtone spectra of methyl halides: A local mode analysis of the spectra of methyl halides and methyl cyanide. J. Chem. Phys. 1987; 87:3724–30.

[66] Badger RM, Bauer SH. Remarks on the spectra of methyl cyanide and methyl isocyanide. J. Chem. Phys. 1937; 59:303–5.

[67] Smith AM, Coy SL, Klemperer W, Lehmann KK. Fourier transform spectra of overtone bands of HCN from 5400 to 15100 cm^{-1}. J. Mol. Spectr. 1989; 134:134–53.

[68] Herzberg G. Molecular spectra and molecular structure II: Infrared and Raman spectra of polyatomic molecules. Princeton: D. Van Nostrand Company Inc.; 1945.

[69] Priestley MB., Spectral Analysis and Time Series. Academic Press, Harcourt Brace & Company Publishers, London; 1981.

TABLES

Table 1 Possible overtone and combination bands (three quanta) of CH_3CN in the region between 5900 and 7500 cm-1. Values have been calculated using the frequencies of the fundamental vibrations of CH_3CN [62] and are only indicative of potential contributions in the spectrum.

Combination Band	Symmetry	Wavenumber [cm^{-1}]
$2\nu_1$	a_1	~5908
$\nu_1 + \nu_5$	e	~5963
$2\nu_5$	a_1	~5908
$\nu_2 + \nu_4 + \nu_5$	e	~6196
$\nu_1 + \nu_2 + \nu_7$	e	~6262
$2\nu_1 + \nu_8$	e	~6270
$\nu_2 + \nu_5 + \nu_7$	a_1	~6317
$\nu_1 + \nu_5 + \nu_8$	a_1	~6325
$2\nu_5 + \nu_8$	e	~6379
$\nu_2 + \nu_3 + \nu_5$	e	~6661
$\nu_1 + \nu_2 + \nu_6$	e	~6669
$\nu_2 + \nu_5 + \nu_6$	a_1	~6724
$3\nu_2$	a_1	~6801
$2\nu_1 + \nu_4$	a_1	~6828
$\nu_1 + \nu_4 + \nu_5$	e	~6883
$\nu_4 + 2\nu_5$	e	~6938
$2\nu_1 + \nu_7$	e	~6949
$\nu_1 + \nu_5 + \nu_7$	e	~7004
$2\nu_5 + \nu_7$	e	~7059
$2\nu_1 + \nu_3$	a_1	~7293
$\nu_1 + \nu_3 + \nu_5$	e	~7348
$2\nu_1 + \nu_6$	e	~7356
$\nu_3 + 2\nu_5$	a_1	~7403
$\nu_1 + \nu_5 + \nu_6$	a_1	~7411
$2\nu_5 + \nu_6$	e	~7446
$\nu_1 + 2\nu_2$	a_1	~7488
$2\nu_2 + \nu_5$	e	~7543

Table 2 Relevant recurring wavenumber differences in spectral regions between 6876 and 7054 cm^{-1} identified by autocorrelation (Column 2) of the absorption signal in the corresponding region and by visual inspection of the spectrum (Column 3).

No.	Spectral region	Autocorrelation $\Delta\tilde{\nu}$ [cm^{-1}]	Observed series $\Delta\tilde{\nu}'$ [cm^{-1}]
1	6876 – 6885	0.68 ± 0.04	0.66 ± 0.02
2	6876 – 6885	1.30 ± 0.06	1.32 ± 0.04
3	6865 – 6871	0.51 ± 0.04	0.57 ± 0.02
4	6865 – 6871	1.22 ± 0.04	1.13 ± 0.04
5	7027 – 7032	0.18 ± 0.06	0.195 ± 0.005
6	7027 – 7032	0.44 ± 0.06	0.430 ± 0.007
7	7027 – 7032	0.62 ± 0.07	0.626 ± 0.005[a]
			0.627 ± 0.006[b]
8	7027 – 7032	0.80 ± 0.05	–
9	7049 – 7054	0.26 ± 0.05	0.26 ± 0.03[c]
			0.33 ± 0.02[d]
10	7049 – 7054	0.58 ± 0.06	0.600 ± 0.003[e]
			0.610 ± 0.003[f]
11	7049 – 7054	0.95 ± 0.04	–

Fig. 1. Structure and molecular coordinate system (a, b, c) of methyl cyanide. This symmetric top molecule has moments of inertia $I_c = I_b$ (= 9.122845×10^{-46} m^2 kg [1]) > I_a (= 5.308074×10^{-47} m^2 kg [2]).

Fig. 2. Reflectivity spectrum of mirrors used for FT-IBBCEAS (upper traces) and off-axis CEAS (lower traces). Trace without error bars (blue): Mirror reflectivity measured with double beam absorption spectrometer (Lambda1050, Perkin-Elmer). Solid and hollow dots: reflectivity values established via calibration with CO_2 at 13.3 mbar and 4 mbar, respectively. Trace with error bars (red): Data obtained with the double beam spectrometer scaled to the average of the CO_2 calibration data (these traces were used as the mirror reflectivity). Error bars correspond to the 1σ standard deviation of the respective calibration data (the point in brackets was left out).

Fig. 3. Left axis (Black trace): Cavity-enhanced absorption spectrum of CH_3CN between 6000 and 8000 cm^{-1} measured by FT-IBBCEAS with a resolution of 0.12 cm^{-1} at a pressure of 4 mbar (data file in supplementary electronic material). Acquisition time 60 min. (Green trace): Region addressed by high resolution off-axis CEAS – section III.*B*. Right axis (Blue trace): "Stick spectrum" of integrated cross-sections of H_2O according to the HITRAN database [54].

Fig. 4. Absorption spectrum of CH_3CN at 4 mbar in the region between 7500 and 8000 cm^{-1} measured at 0.12 cm^{-1} resolution using FT-IBBCEAS. Only absorption to states consisting of four vibrational quanta contributes to the spectrum in this region. SNR is approximately 60.

Fig. 5. Off-axis cavity-enhanced absorption spectrum of CH_3CN between 6814 and 7067 cm^{-1} measured at a pressure of 5 mbar. There are ~4630 new absorption transitions in this spectrum; water features were removed. Approximately 200 individual overlapping spectral segments were concatenated to cover the spectral range shown (data file in supplementary electronic material).

Fig. 6. A 10 cm^{-1} section of the CH_3CN spectrum illustrating the importance of the removal of water absorption features. Upper trace (left axis): Fourier transform detection, resolution 0.12 cm^{-1}. Lower trace (left axis): off-axis CEAS detection, resolution 0.001 cm^{-1}. Stick spectrum (right axis, blue): H_2O reference values obtained from the HITRAN database [54].

Fig. 7. Upper panel (a): Arbitrarily *J*-numbered series of seemingly equidistant absorption lines in the region between 6865 and 6871 cm^{-1}. Middle panel (b): Autocorrelation analysis of the spectral region between 6876 and 6885 cm^{-1}.

The two peaks highlighted by vertical arrows can be related to wavenumber differences in the spectrum. Lower panel (c): Peak positions versus relative (arbitrary) values of *J* with associated linear (red) and 2nd order polynomial (blue) fits. Lower panel: residuals of linear (red) and 2nd order polynomial fits (blue).

Fig. 8. One of several unresolved band heads in the spectral region around 6993 cm^{-1}.

Fig. 9. Lorentzian FWHM of the absorption line at 7034.17 cm^{-1} as a function of pressure. Dashed line: Linear regression. Red line: linear regression forced through origin. Insert: Example of a fit of Voigt function to the absorption line measured at 5 mbar resulting in $FWHM_{Gauss}$=0.0126 cm^{-1} and $FWHM_{Lorentz}$=0.0144 cm^{-1} and residuals in the lower panel of the insert.

Supplementary material

Data shown in Fig. 3

Data shown in Fig. 5

Figure 1

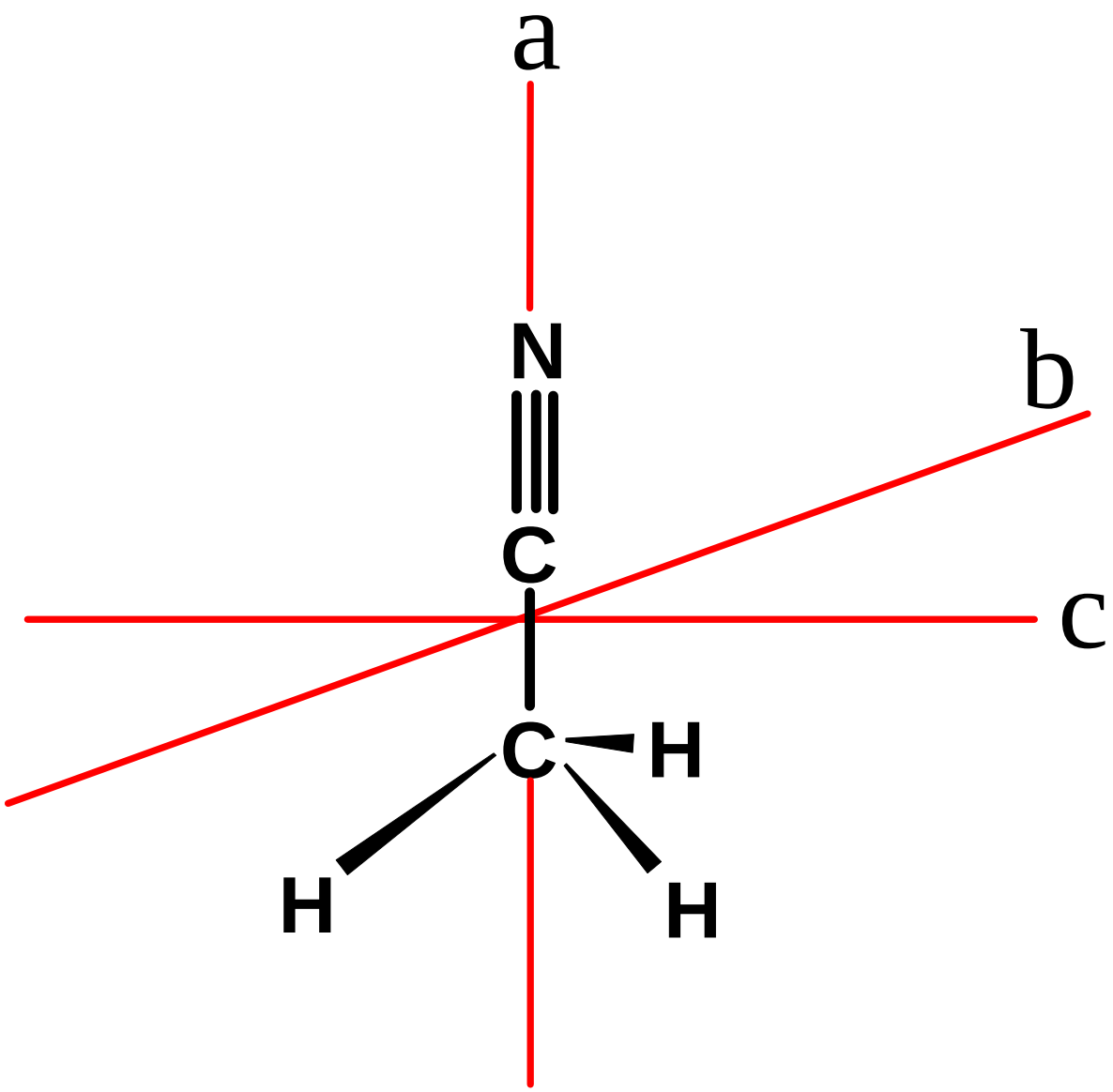

Figure 2

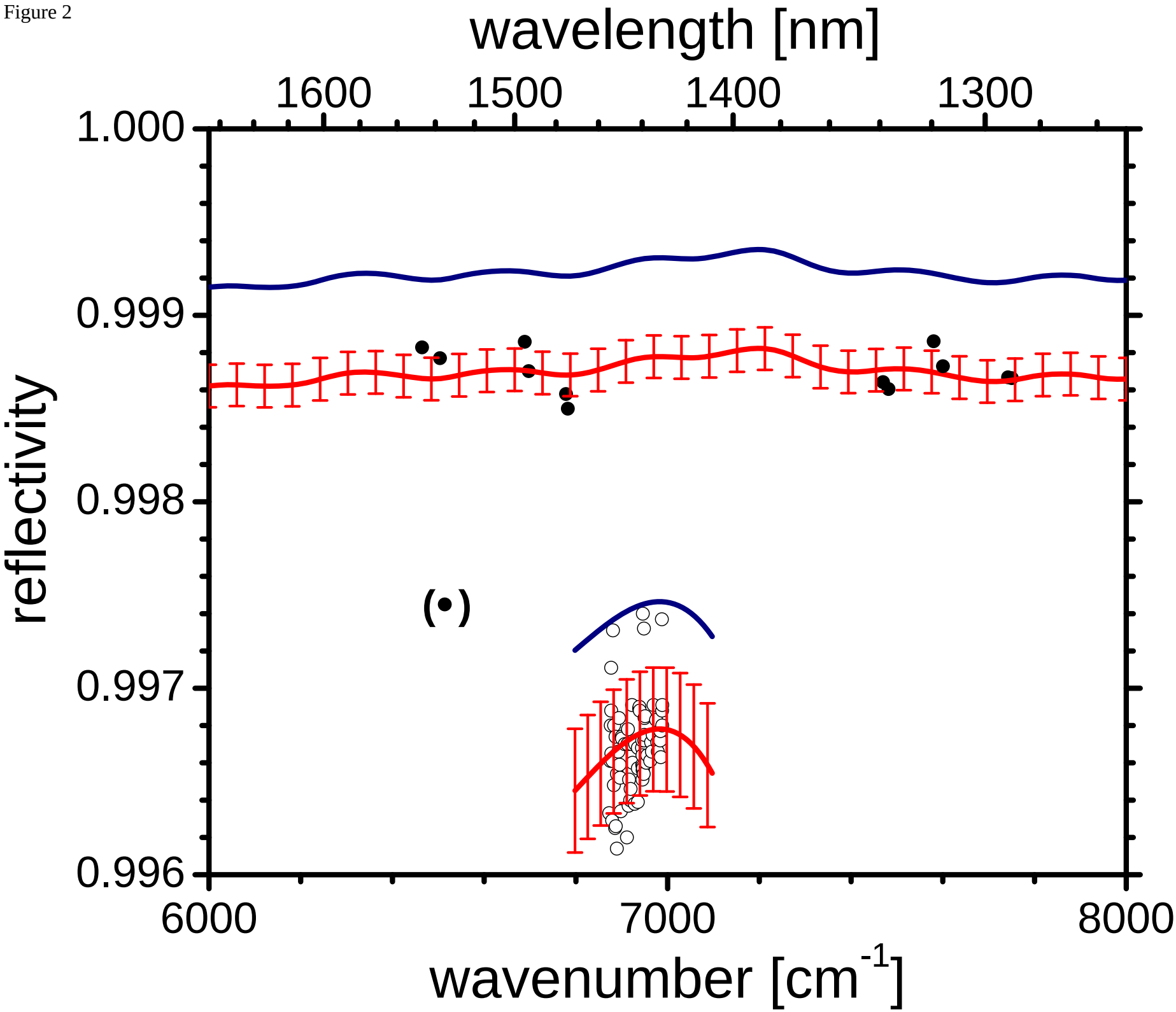
wavelength [nm]
1600
1500
1400
1300
1.000
0.999
0.998
0.997
0.996
reflectivity
(•)
6000
7000
8000
wavenumber [cm-1]

Figure 3

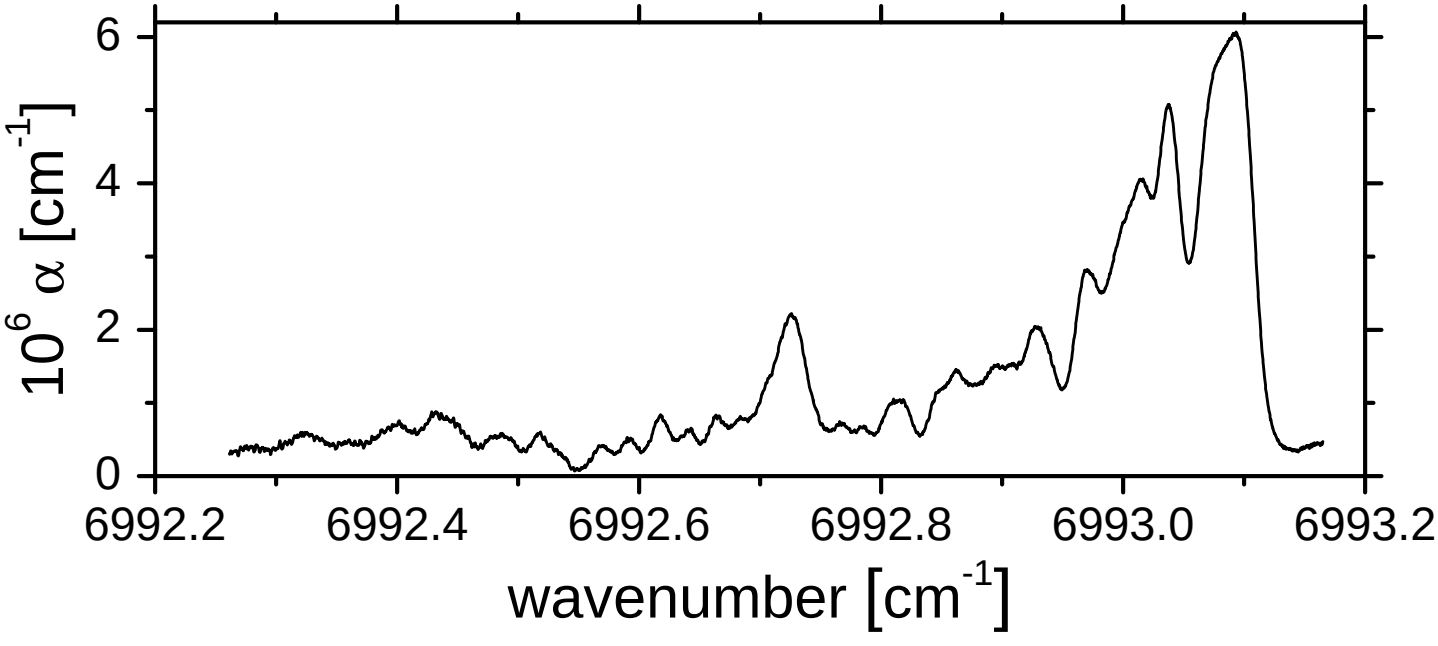
6
4
2
0
10^6 α [cm^{-1}]
6992.2
6992.4
6992.6
6992.8
6993.0
6993.2
wavenumber [cm^{-1}]

Figure 4

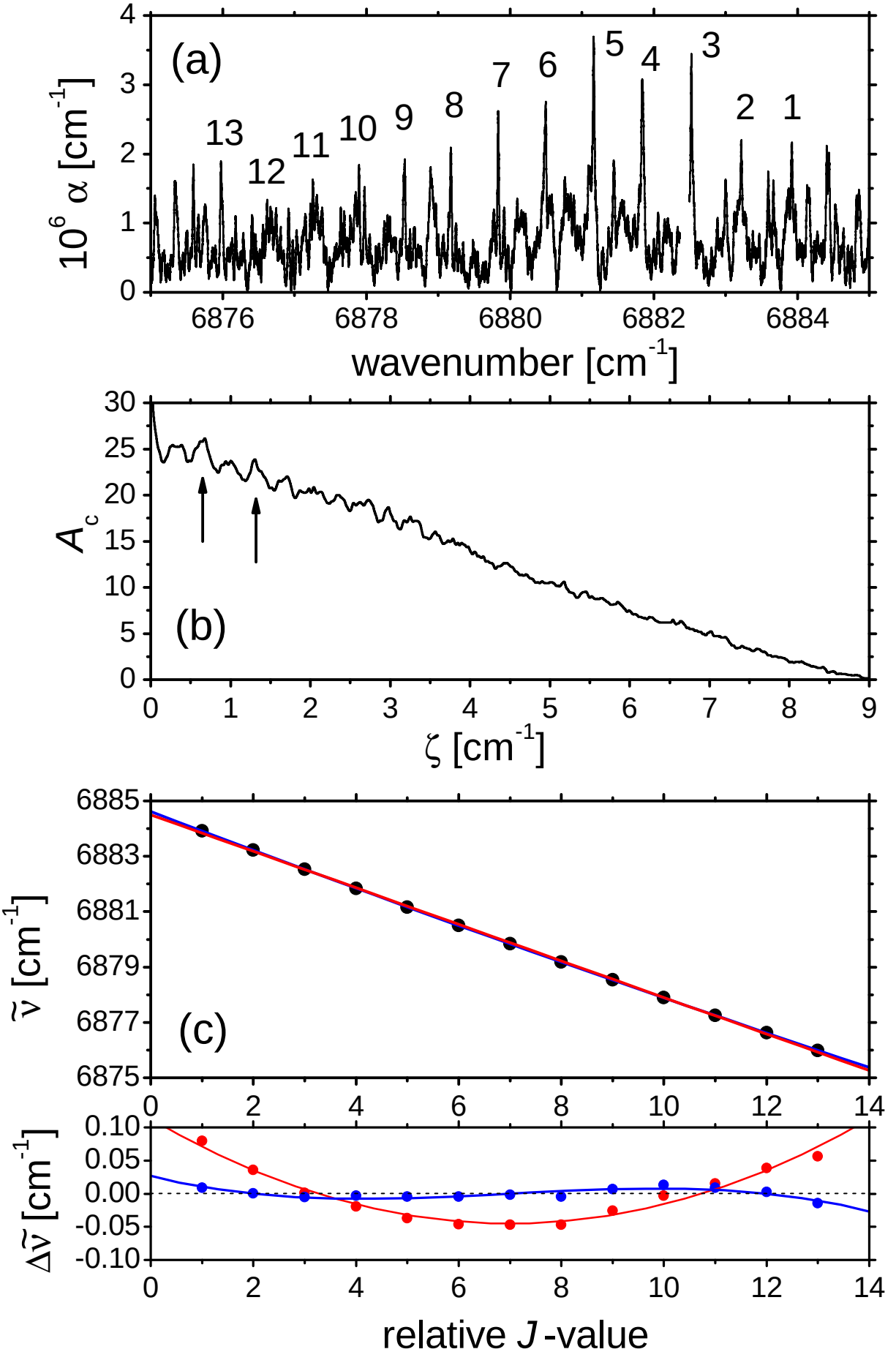
(a)
$10^6\ \alpha\ [cm^{-1}]$
13
12
11
10
9
8
7
6
5
4
3
2
1
wavenumber [cm^{-1}]
(b)
A_c
$\zeta\ [cm^{-1}]$
(c)
$\tilde{\nu}\ [cm^{-1}]$
$\Delta\tilde{\nu}\ [cm^{-1}]$
relative J-value

Figure 5

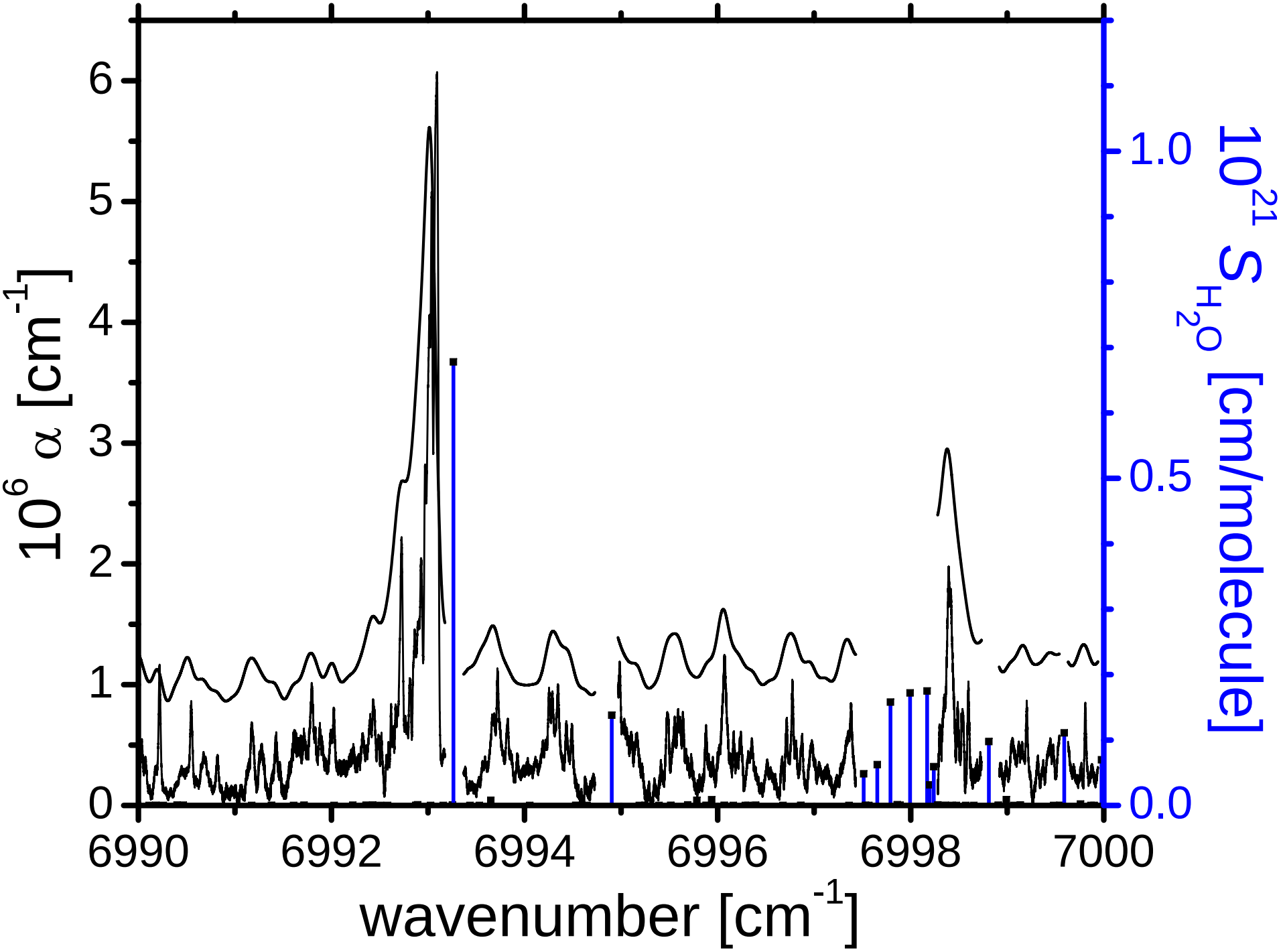
6
5
4
3
2
1
0
10^6 α [cm^{-1}]
1.0
0.5
0.0
10^{21} S_{H_2O} [cm/molecule]
6990
6992
6994
6996
6998
7000
wavenumber [cm^{-1}]

Figure 6

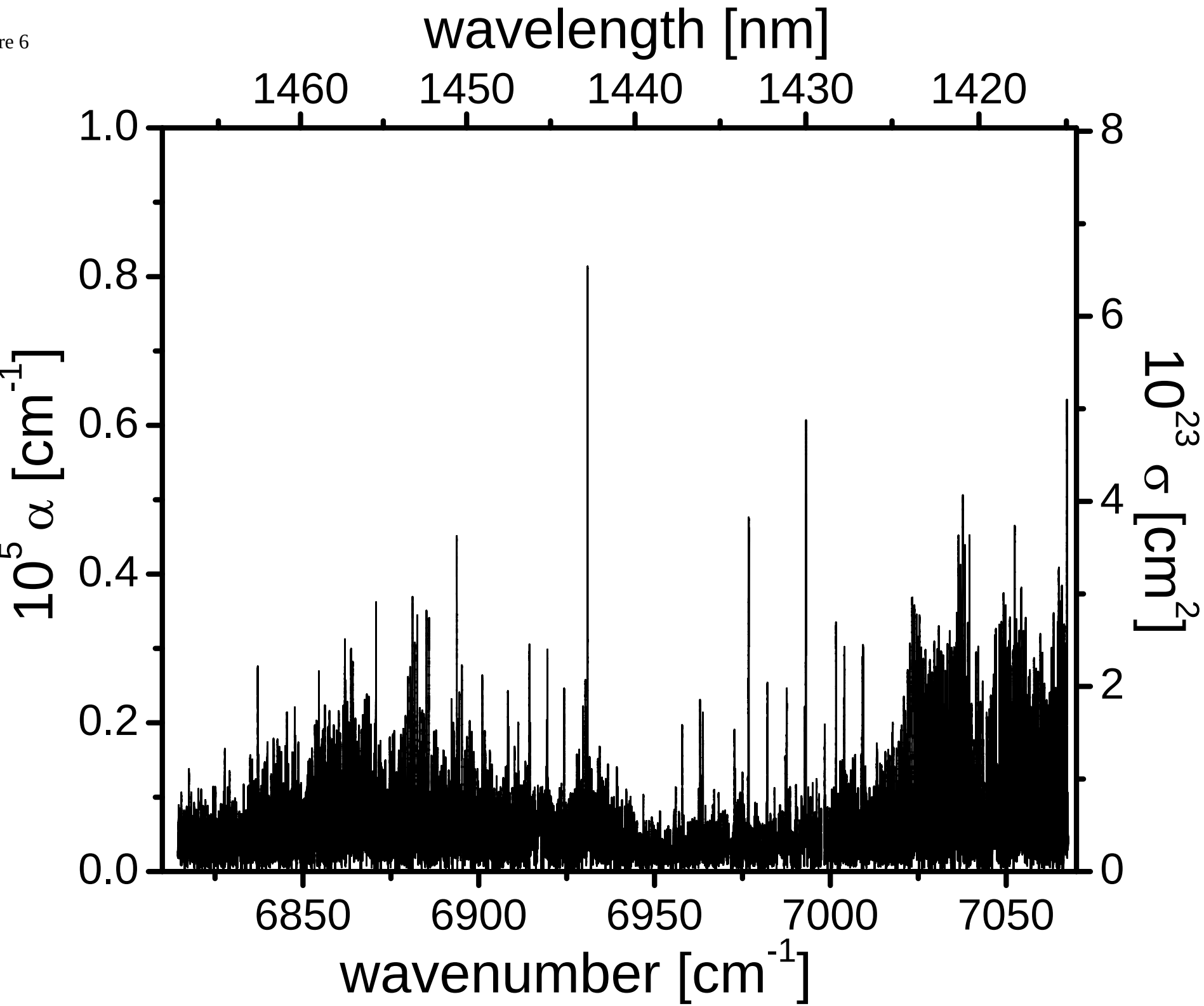
wavelength [nm]
1460
1450
1440
1430
1420
1.0
0.8
0.6
0.4
0.2
0.0
8
6
4
2
0
$10^5 \alpha$ [cm^{-1}]
$10^{23} \sigma$ [cm^2]
6850
6900
6950
7000
7050
wavenumber [cm^{-1}]

Figure 7

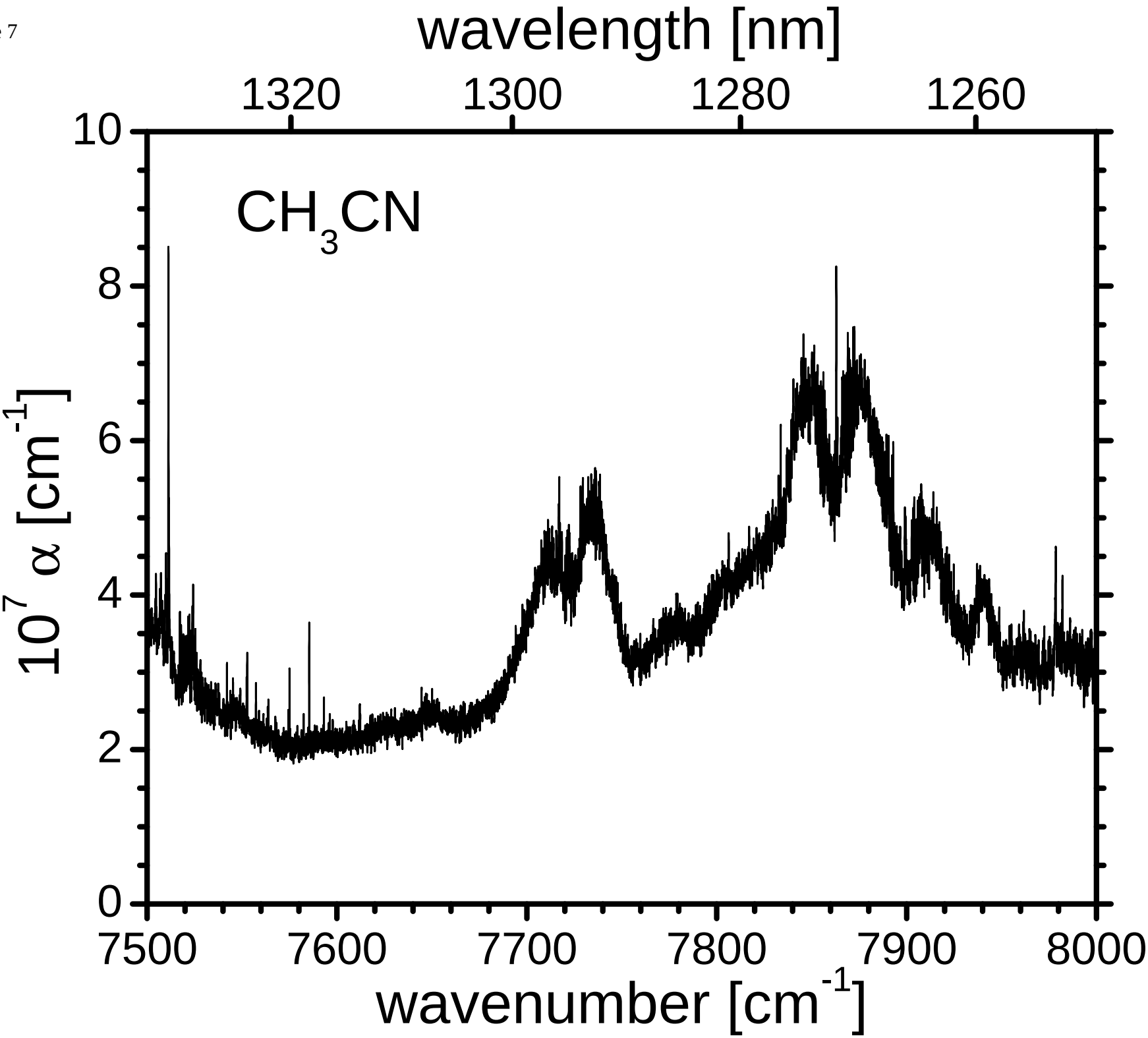
wavelength [nm]
1320
1300
1280
1260
CH3CN
10
8
6
4
2
0
10^7 α [cm^-1]
7500
7600
7700
7800
7900
8000
wavenumber [cm^-1]

Figure 8

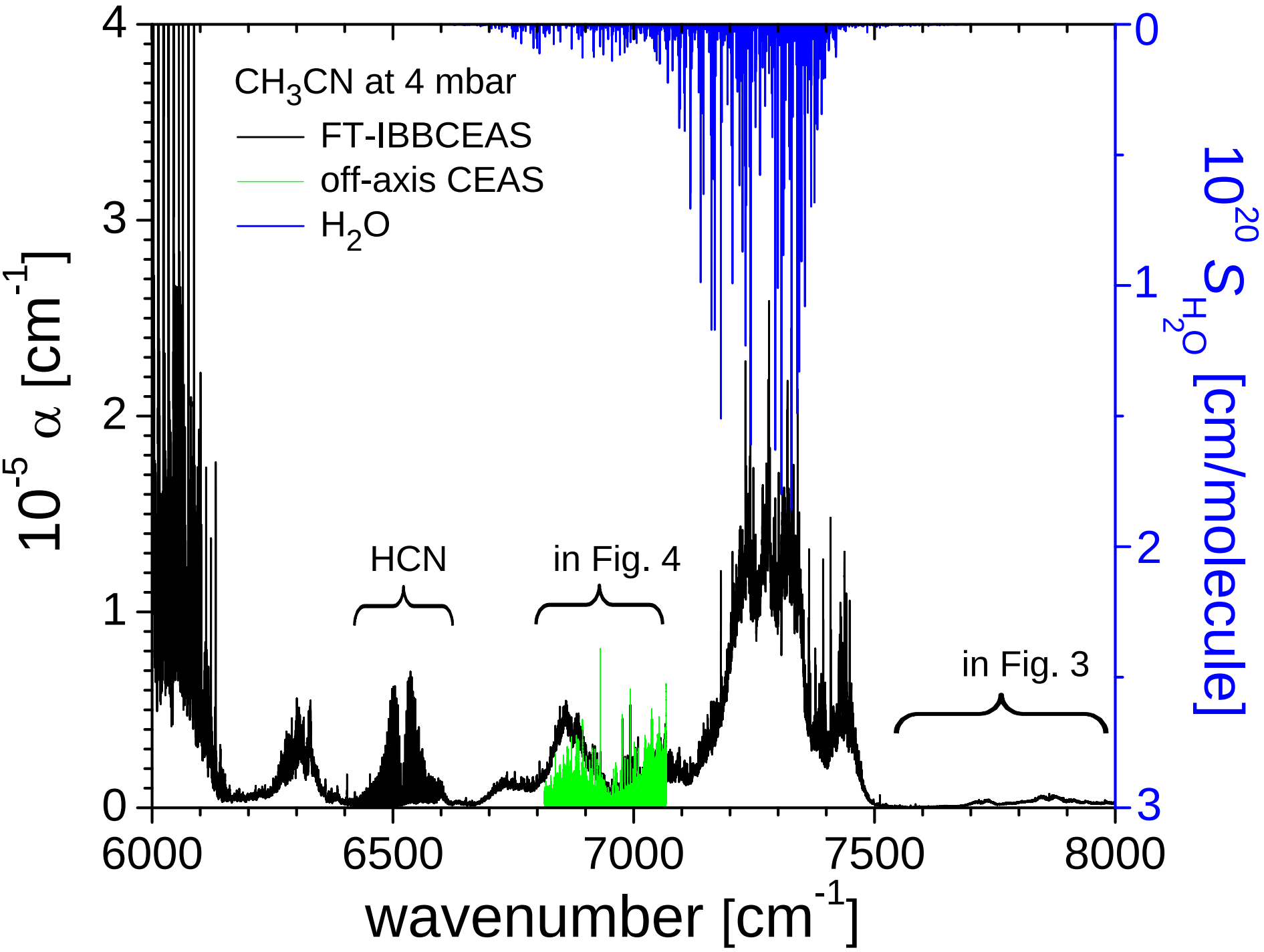
CH3CN at 4 mbar
FT-IBBCEAS
off-axis CEAS
H2O
HCN
in Fig. 4
in Fig. 3
10-5 α [cm-1]
10^20 S H2O [cm/molecule]
wavenumber [cm-1]
0
1
2
3
4
6000
6500
7000
7500
8000

Figure 9

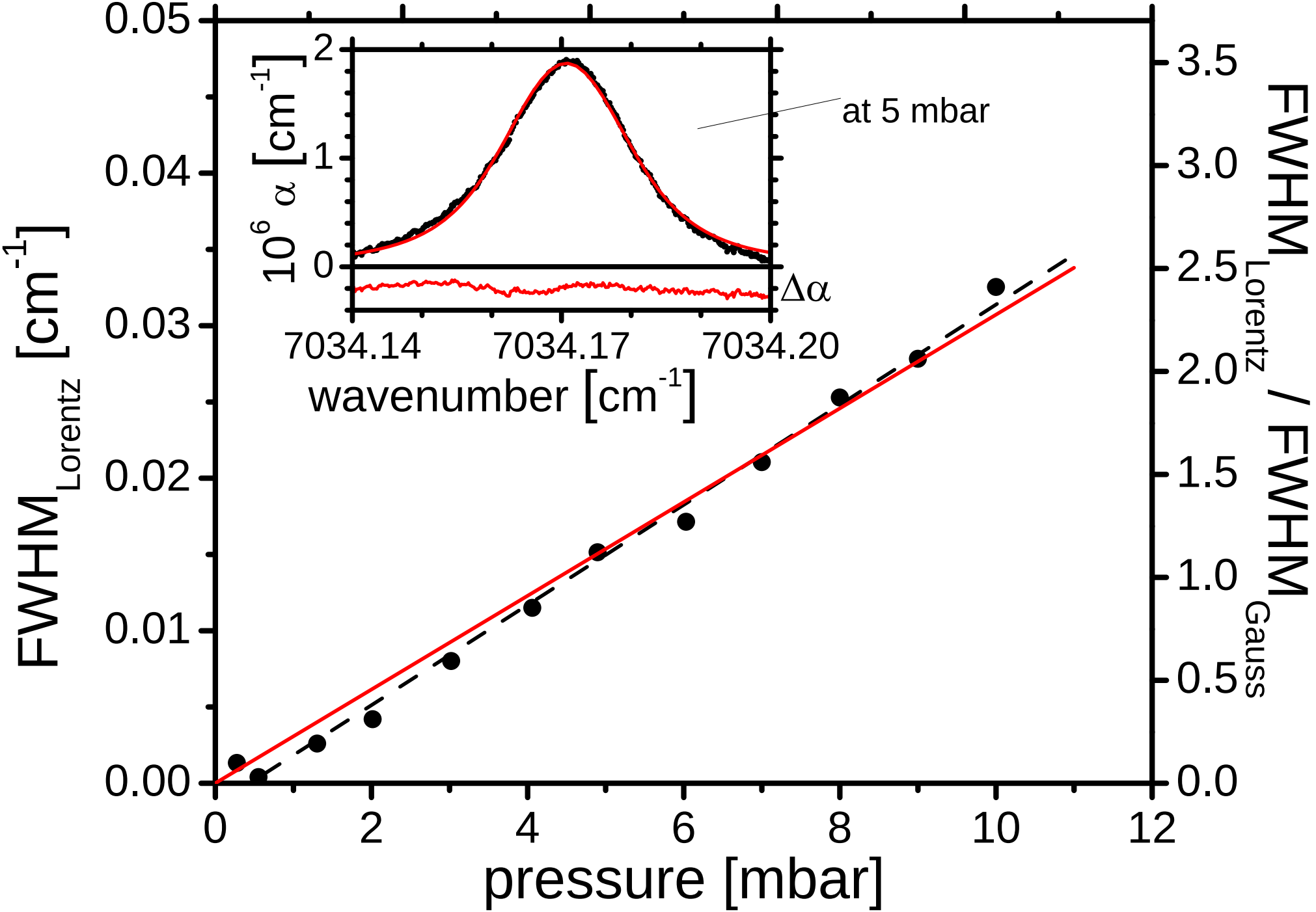
0.05
0.04
0.03
0.02
0.01
0.00
FWHM Lorentz [cm-1]
0
2
4
6
8
10
12
pressure [mbar]
3.5
3.0
2.5
2.0
1.5
1.0
0.5
0.0
FWHM Lorentz / FWHM Gauss
2
1
0
10^6 α [cm-1]
at 5 mbar
Δα
7034.14
7034.17
7034.20
wavenumber [cm-1]